O+C analysis @GSI2021: paper

Riccardo Ridolfi

17 December 2024 - XVII FOOT Collaboration Meeting

Paper organization overview

Angular differential and elemental fragmentation cross sections of a ^{16}O beam on a graphite target with the FOOT experiment

I. Introduction
II. Experimental Setup
III. Data Analysis
IV. Results
V. Conclusions

References

The target journal is <u>PRC</u>

I. INTRODUCTION

Nuclear fragmentation cross section measurements are crucial for advancing in several fields, such as Particle Therapy (PT), Radioprotection in Space (RPS) and nuclear structure [1, 2]. For instance, in PT understanding the fragmentation of ion beams as they interact with human tissue is essential to improve cancer treatments, as it helps in accurately predicting the dose distribution and minimizing damage to surrounding healthy tissues [3, 4]. Moreover, an accurate description of fragmentation phenomena can also shed light on the biological effectiveness in proton therapy [5].

Similarly, in RPS these measurements would be of paramount importance for assessing the risks posed by cosmic radiation to astronauts, as they help in developing effective shielding strategies [6]. Indeed, the health risks related to the space radiation still remain one of the major risks for space exploration beyond Low Earth Orbit (LEO) which is among future plans of several national space agencies and private companies [7]. These hazards could be so important to prevent space missions due to huge costs and unacceptable risks for the astronauts given the lack of effective countermeasures so far [8].

These fields share a common ground both for ions involved (from ^{1}H to ^{56}Fe with a focus on ions with nuclear charge number $Z \leq 8$) and kinetic energies (depending on the ion, in the range $100 - 1000$ MeV/u). However, the phenomena at play are known with poor accuracy due to the lack or the poor precision of the relevant fragmentation cross section measurements [9–11]. This translates in a poor precision in the computation of the dose due to the fragments with respect to the one required for both PT and RPS applications [12, 13]. The measurement of the missing fragmentation cross sections would allow to benchmark and update the existing nuclear models implemented in Monte Carlo (MC) and deterministic codes, used for the dose computation in both the PT and RPS applications [14, 15].Double differential cross sections in the fragment production angle and kinetic energy would be of great value to this purpose. In the last years some of the missing fragmentation cross sections have been measured, but still very few beam-target-energy combinations have been explored [16–21].

The FOOT experiment [22] has been designed to address the significant lack of data needed in these fields by measuring fragmentation cross sections in the nuclear interactions between ion beams (such as protons, Helium, Carbon, and Oxygen) and targets of interest for PT, like H C and O, which are the most abundant elements in the human tissues, and targets of interest for shielding in RPS like hydrogen-enriched targets [22].

FOOT is a fixed target experiment whose setup includes two complementary and alternative configurations: an electronic setup with a magnetic spectrometer along with charge and mass identification capabilities, dedicated to the measurement of the forward emitted fragments with $Z > 2$, and an emulsion spectrometer for higher angular acceptance measurements of the light fragments with $Z < 3$. Details of the FOOT experiment design and some preliminary results can be found in [22–27].

The data analyzed in this paper were among those acquired at the GSI Helmholtz Center of Heavy Ion Research facility in Darmstadt in 2021 with the electronic setup. At that time only a part of the final FOOT detector, as described in detail in [22], was already developed. The setup, consisting of a detector for the beam monitoring and a system for the Time-of-Flight and the energy loss measurements, was used to identify the charge Z of the fragments and to measure their emission angle allowing to perform elemental cross section measurements. The same setup was used in a previous data acquisition in 2019 in GSI, described in detail in [23].

In this paper, the measurement of the angular differential cross sections for the forward production of $2 \leq Z \leq 7$ nuclei in the fragmentation process of a 400 MeV/u ^{16}O beam interacting with a graphite target will be presented. This contribution aims at extending in terms of statistics and results those already published with the 2019 data taking [23] , where a limited statistics allowed to measure only elemental fragmentation cross section integrated in the full geometrical acceptance of the setup. In this data analysis, thanks to a factor more than 100 in the available statistics, with respect to the 2019 data campaign, it was possible to measure, for the first time for FOOT, the angular differential cross section for charged fragments production. In Sec. II the FOOT setup used in the analysis will be discussed, in Sec. III firstly the analysis strategy will be described, then the Monte Carlo simulation framework together with purity corrections for charge identification, the unfolding procedure for angular measurements and efficiency corrections for fragment reconstruction will be outlined. Eventually, a comprehensive assessment of systematic uncertainties from detector effects and the analysis method will be

Applications Context

Scientific Gap

FOOT Experiment Overview

Purpose of the paper

I. INTRODUCTION

Nuclear fragmentation cross section measurements are crucial for advancing in several fields, such as Particle Therapy (PT), Radioprotection in Space (RPS) and nuclear structure [1] [2]. For instance, in PT understanding the fragmentation of ion beams as they interact with human tissue is essential to improve cancer treatments, as it helps in accurately predicting the dose distribution and minimizing damage to surrounding healthy tissues [3] [4]. Moreover, an accurate description of fragmentation phenomena can also shed light on the biological effectiveness in proton therapy [5].

Similarly, in RPS these measurements would be of paramount importance for assessing the risks posed by cosmic radiation to astronauts, as they help in developing effective shielding strategies [6]. Indeed, the health risks related to the space radiation still remain one of the major risks for space exploration beyond Low Earth Orbit (LEO) which is among future plans of several national space agencies and private companies [7]. These hazards could be so important to prevent space missions due to huge costs and unacceptable risks for the astronauts given the lack of effective countermeasures so far [8].

These fields share a common ground both for ions involved (from ^{1}H to ^{56}Fe with a focus on ions with nuclear charge number $Z \leq 8$) and kinetic energies (depending on the ion, in the range $100 - 1000$ MeV/u). However, the phenomena at play are known with poor accuracy due to the lack or the poor precision of the relevant fragmentation cross section measurements [9]-[11]. This translates in a poor precision in the computation of the dose due to the fragments with respect to the one required for both PT and RPS applications [12] [13]. The measurement of the missing fragmentation cross sections would allow to benchmark and update the existing nuclear models implemented in Monte Carlo (MC) and deterministic codes, used for the dose computation in both the PT and RPS applications [14] [15].Double differential cross sections in the fragment production angle and kinetic energy would be of great value to this purpose. In the last years some of the missing fragmentation cross sections have been measured, but still very few beam-target-energy combinations have been explored [16]-[21].

The FOOT experiment [22] has been designed to address the significant lack of data needed in these fields by measuring fragmentation cross sections in the nuclear interactions between ion beams (such as protons, Helium, Carbon, and Oxygen) and targets of interest for PT, like H C and O, which are the most abundant elements in the human tissues, and targets of interest for shielding in RPS like hydrogen-enriched targets [22].

FOOT is a fixed target experiment whose setup includes two complementary and alternative configurations: an electronic setup with a magnetic spectrometer along with charge and mass identification capabilities, dedicated to the measurement of the forward emitted fragments with $Z > 2$, and an emulsion spectrometer for higher angular acceptance measurements of the light fragments with $Z < 3$. Details of the FOOT experiment design and some preliminary results can be found in [22]-[27].

The data analyzed in this paper were among those acquired at the GSI Helmholtz Center of Heavy Ion Research facility in Darmstadt in 2021 with the electronic setup. At that time only a part of the final FOOT detector, as described in detail in [22], was already developed. The setup, consisting of a detector for the beam monitoring and a system for the Time-of-Flight and the energy loss measurements, was used to identify the charge Z of the fragments and to measure their emission angle allowing to perform elemental cross section measurements. The same setup was used in a previous data acquisition in 2019 in GSI, described in detail in [23].

In this paper, the measurement of the angular differential cross sections for the forward production of $2 \leq Z \leq 7$ nuclei in the fragmentation process of a 400 MeV/u ^{16}O beam interacting with a graphite target will be presented. This contribution aims at extending in terms of statistics and results those already published with the 2019 data taking [23] , where a limited statistics allowed to measure only elemental fragmentation cross section integrated in the full geometrical acceptance of the setup. In this data analysis, thanks to a factor more than 100 in the available statistics, with respect to the 2019 data campaign, it was possible to measure, for the first time for FOOT, the angular differential cross section for charged fragments production. In Sec. II the FOOT setup used in the analysis will be discussed, in Sec. III firstly the analysis strategy will be described, then the Monte Carlo simulation framework together with purity corrections for charge identification, the unfolding procedure for angular measurements and efficiency corrections for fragment reconstruction will be outlined. Eventually, a comprehensive assessment of systematic uncertainties from detector effects and the analysis method will be

Overall setup description

Individual detector component

Detection strategy

reported. In Sec. IV the results of the paper will be discussed taking into account previous results both from other researches and from previous works of the FOOT experiment [23] with a focus on the improvements enabled by higher statistics and enhanced analysis techniques.

II. EXPERIMENTAL SETUP

The experimental setup used in the data campaign analyzed in this paper is identical to the one used in the GSI 2019 data taking campaign and described in detail in [23] (see Figure 1). The fragmentation due to the interaction of a ^{16}O beam of 400 MeV/u with a 5 mm graphite target (TG) is studied. The two detectors upstream the graphite target, the Start Counter (SC) and the Beam Monitor (BM) are meant to monitor the beam. Their design minimize the pre-target overall material budget in order to keep the internal fragmentation inside themselves at the percentage level with respect to the one in the target. The only detector downstream the target is the TOF-Wall (TW) a hodoscope composed of two layers of scintillator bars, able to provide identification of the charge Z of the fragments [23].

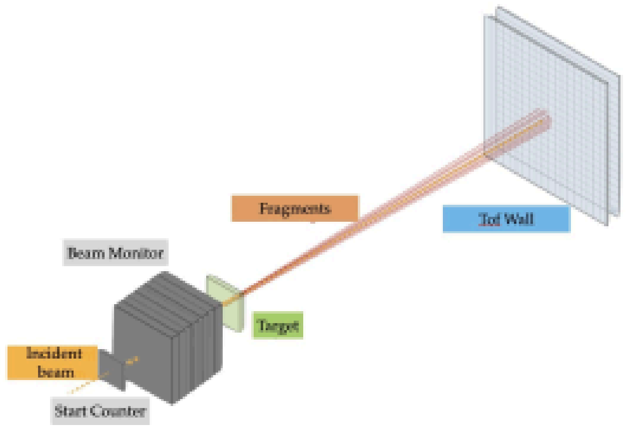

FIG. 1. Schematic view of the GSI experimental setup. The ^{16}O beam passes through the Start Counter and the Beam Monitor, before impinging on the 5 mm thick graphite target. The produced fragments emitted with a polar angle $\leq 5.7^{\circ}$ can be identified by the Tof-Wall detector, about 190 cm downstream of the target [23].

The Start Counter (SC) [28] is a 250 µm thick plastic scintillator (EJ-228), placed at the very beginning of the setup, which is aimed to measure the incoming ion flux and provides time measurement with a resolution of $\sim$ 70 ps for ^{16}O ions [29]. The Beam Monitor (BM) is a drift chamber consisting of twelve wire layers, with X-Y view. With a tracking efficiency higher than 90% and a lower limit on the spatial resolution of 60 µm [30] it provides the measurement of the direction and the interacting point of the beam ions on the target. The distances between SC, BM and TG have been minimized as much as possible. This choice minimizes the effects of the multiple scattering and maximizes the position resolution on the BM track projection on the TG.

The ToF Wall detector (TW) is a hodoscope composed of two layers of 20 plastic scintillator bars (EJ-200) each, arranged orthogonally to provide X-Y view. The two orthogonal x-y layers form a $40 \times 40\,\mathrm{cm}^2$ active area detector that provides the measurements of the energy deposited ΔE, with a resolution of $\sigma(\Delta E)/\Delta E \sim 5$ %, the stop time, with a resolution of ~ 20 ps for ^{16}O ions [29] to compute the TOF (the start time is provided by the SC), and the hit position with the granularity provided by the bar crossing dimension of 2×2 cm^2. Because most of the fragments, with the exception of protons and neutrons, according to MC and previous measurement [15, 22], are forward emitted within a maximum angle of 10° for He, the TW was moved $\sim$ 190 cm downstream the target in order to maximize its full surface for most of the fragments. At the same time the chosen distance minimize events with multiple fragments within the TW granularity (provided by the bar crossing of 2×2 cm^2). According to a MC simulations the chosen granularity keeps the pile-up of multiple fragments in the same bars' cross below 1% [22, 23]. The TW detector is not optimized for protons and neutrons detection which for this reason are excluded by the analysis. The TW dimension and distances from the target set the geometrical acceptance of the setup. Taking into account also a 1 cm x-y shift between the center of the upstream region (SC, BM and TG) with respect to the one of the TW, the polar angle acceptance for this analysis is $\leq 5.7°$.

The simultaneous measurement of the ΔE in a TW bar and the TOF between that bar and the SC allows to identify the charge Z of the ion crossing the TW. As detailed in [23], from a parametrization with a Bethe-Bloch curve of the ΔE as a function of ToF, for each TW layer, the charge Z of each fragment is extracted. Whenever a fragment cross the TW, pairs of crossed X-Y bars sharing the same reconstructed Z are clusterized in a TW point, with a position resolution provided by the bar crossing of 2×2 cm^2. The fragment hit position along the bar, extracted with the time difference measured at both the edges of a single bar, is used to improve the clusterization of the X-Y bars forming a TW point [23]. In order to show the separation of the different fragments' charge Z in Fig. 2 the Bethe-Bloch curves used for the charge Z identification of the fragment are superimposed to the distribution of ΔE vs the TOF for each reconstructed TW point. Data are from the sample collected in 2021 at the GSI facility, analyzed in this work.

III. DATA ANALYSIS

The data analyzed in this paper were collected during the FOOT data taking campaign at GSI in 2021, with the setup reported in the previous Sec. II. Two different samples of data were collected: a sample with a ^{16}O beam

Summary of available data

Cross section formula

Background subtraction

Number of primaries evaluation and integrated cross section

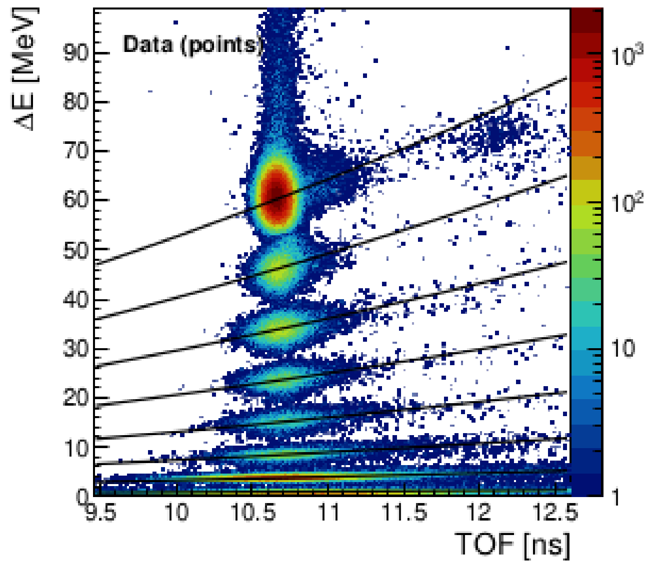

FIG. 2. ΔE vs TOF distribution for the data collected at GSI in 2021, analyzed in this work. The Bethe-Bloch curves are superimposed. The separation between the different fragment charge Z releases is visible

of 400 MeV/u impinging on a 5 mm carbon target and another acquired without target in order to take into account the fragmentation coming from the interaction of the beam with the air and the FOOT setup, to be considered as a background in the cross section analysis.

Data were acquired using two different trigger strategies: the Minimum Bias (MB) trigger is issued whenever a primary ion of ^{16}O goes through the SC , while the fragmentation trigger (FRAG) purpose is to reject most of the primaries events reaching the TW, acquiring mostly fragmentation events of interest for cross section measurement.

About 1.2×10^6 events were acquired with the MB trigger implemented requiring in the SC a majority of 5 of its readout channels over the total of 8 [28, 31]. About 2×10^6 events were acquired with the FRAG trigger, able to reject most of the ^{16}O reaching the TW, requiring a coincidence of a MB trigger with a veto from events with an energy release in the TW central bars compatible with a primary ion of the beam [31]. In both cases the data were acquired with the TG. About 5×10^5 events were acquired with the MB trigger for the sample without target, for background studies.

The goal of this analysis is to evaluate the angular differential cross sections for the fragmentation process of a ^{16}O beam of 400 MeV/u interacting with a graphite target . No detectors providing the momentum or the kinetic energy of the produced fragments are present in the setup (Sec. II) and so mass identification is not feasible and only elemental fragmentation cross sections can be measured. The angular differential fragmentation cross sections for the forward production ($\theta \leq 5.7°$) of He, Li, Be, B, C and N nuclei will be presented. The elemental cross section for each fragment charge Z is computed as follow

$$\frac{d\sigma}{d\Omega}(Z) = \frac{Y(Z,\theta)}{N_{\rm prim} \cdot N_{\rm TG} \cdot \varepsilon(Z,\theta) \cdot \Delta\Omega} \qquad (1)$$

where $Y(Z,\theta)$ is the number of fragments of a given charge Z measured by TW at a given angle θ, $N_{\rm prim}$ is the number of primaries impinging on the target, $\varepsilon(Z,\theta)$ is the efficiency for a given charge in a given angle computed using a MC simulation (see Sec. III A and III D), $\Delta\Omega$ is the solid angle bin width and $N_{\rm TG}$ is the number of interaction centers in the target per unit surface which can be written as

$$N_{\rm TG} = \frac{\rho \cdot \Delta x \cdot N_{\rm A}}{A} \qquad (2)$$

where $\rho = 1.83\,{\rm g/cm^3}$ is the graphite target density, $\Delta x = 0.5\,{\rm cm}$ is the target thickness, $N_{\rm A}$ is the Avogadro number and $A = 12.0107\,{\rm g/mol}$ is the graphite mass number. Details on how the factors entering in Eq 1 are computed or measured are given below.

In order to measure the fragmentation yields $Y(Z,\theta)$ produced in the target, the out-of-target fragmentation, mostly produced by the interaction of the ^{16}O beam with the air and the FOOT setup, has to be taken into account. This contribution has to be considered as background with respect to the in-target fragmentation and need to be detected and removed. The reconstruction workflow is the same for with and without target samples: firstly, the angle of the primary particle and its impact point on the target is calculated by the BM. Then, the angle between the impact point on target and the reconstructed point on the TW is calculated, and the charge Z of the fragment is identified by the TW. Since the TW cannot distinguish whether fragments come from the target or not, all the valid points are taken into account and their emission angle is calculated as pointed out above even if fragments are not generated in the target. The background which arises from these wrong reconstructions is removed using the without target sample. In conclusion the quantity $Y(Z,\theta)/N_{\rm prim}$ of Eq. (1) can be rewritten as

$$\frac{Y(Z,\theta)}{N_{\rm prim}} = \frac{Y_{\rm TG}(Z,\theta)}{N_{\rm prim,TG}} - \frac{Y_{\rm noTG}(Z,\theta)}{N_{\rm prim,noTG}} \qquad (3)$$

where the subscript TG (noTG) refers to the runs with (without) the target. In this way, fragment yields are correctly subtracted taking into account the different number of primaries in the two data samples.

The number of primaries, in minimum bias (MB) runs, is the number of events passing the selection cuts on the SC and on the BM. Namely, multiple primary particles in the same event (i.e. pileup events) have to be removed: this can be achieved by looking both at the SC raw signal and at the number of BM reconstructed tracks. The pileup chance mainly depends on the beam rate which can undergo to large variations during data takings: these changes can challenge the BM since its acquisition time window is the largest among the detectors used in this analysis. The cleaning of the pile up events in SC and the request of events with only one BM track reduces the number of MB trigger to be considered for the analysis of 10-12% depending on the average beam rate of each run. Note that these selections are performed before the effective beam passage in the target so that no significant biases are introduced in the analysis.

While for minimum bias (MB) runs the number of primaries is the number of events surviving previous cuts, for fragmentation (FRAG) runs the effect of the trigger selection on the number of primaries has to be evaluated. During MB runs, trigger thresholds for fragmentation trigger, compatible with the energy deposited by a ^{16}O in central TW bars, are set in order to count the number of times the fragmentation trigger conditions are valid during MB runs. By looking at the ratio between the number of events labeled as fragmentation events and their total number it is possible to find the *trigger acceptance factor* which resulted to be $\simeq 16\%$. This number will divide the number of fragmentation trigger events in FRAG runs acting as a scaling factor to properly count the number of primaries in cross section measurements. The selection performed by the trigger should reject mostly primaries not interacting in the setup but some fragments could be cut away resulting in a loss of fragments: however, this contribution was estimated to be negligible with respect to other sources of uncertainty.

The minimum angular bin width used in the cross section (Eq.1) was set taking into account the TW granularity ($\approx 0.57°$ at the target position) while the choice of the number of bins was mainly driven by the available statistics in background data, which dominate the statistical error. The fragmentation cross sections are evaluated in the geometrical acceptance of the apparatus of 5.7°, and in the beta interval $[\beta_{\min}, \beta_{\max}] = [0.3, 0.9]$, extracted from the beta distributions measured in data. Integrating over the angle the Eq. 1 and over the available phase space, the elemental cross section for each charge Z can be extracted as follows:

$$\Delta\sigma(Z) = \int_{\beta_{\min}}^{\beta_{\max}} \int_{\Omega} \left(\frac{\partial^2\sigma}{\partial\Omega\partial\beta}\right) \mathrm{d}\Omega \mathrm{d}\beta =$$

$$= \frac{Y(Z)}{N_{\mathrm{prim}} \cdot N_{\mathrm{TG}} \cdot \varepsilon(Z)} \quad (4)$$

In the present work both the integral and the angular differential cross sections have been measured and will be discussed in the results (see Sec. IV).

A. Monte Carlo simulation

A detailed Monte Carlo (MC) simulation of the setup described in Sec. II was carried out using the FLUKA MC code [32]. The MC simulation was tailored to the detector geometry along with passive materials, shifts and rotations of the setup [33]. Both the setups with the carbon target and without the target were simulated. The ^{16}O beam position and its transverse size were tuned from data and implemented in the MC simulation. Simulation outputs are processed by the FOOT reconstruction software which performs the reconstruction as in data. The reconstruction of the quantities of interest, tracks for BM and points for TW and their performances were already studied and optimized in MC in other works [23, 30]. The detectors experimental responses have been extracted from data and calibration runs dedicated to single detectors and tuned in MC as described elsewhere [23, 28, 30, 34]: spatial resolution in BM and energy loss and Tof resolutions in SC and TW have been tuned in MC applying a Gaussian smearing to the quantities of interest computed with FLUKA. The tuning of the MC on data is fundamental to make the MC reliable for what concern the fragment Z identification (ZID) and the angle of the reconstructed fragments [23], which are the two quantities needed to extract the fragments raw yields for the angular differential cross sections, as discussed in the previous paragraph.

The main purpose of the MC simulation is to compute corrections to the measurement of the fragmentation cross sections (Eq. 1 and (4)). An efficiency correction, detailed in Sec. III D is introduced to correct for the missing fragments, produced in the fragmentation process, but lost in reconstruction. A purity correction, discussed in Sec. III B is introduced to correct the fragmentation yield $Y(Z, \theta)$ to take into account the misidentification of the Z charge due to the ZID algorithm of TW detector.

The analysis strategy shown in the previous paragraph, for the cross section evaluation, was validated against the MC simulation: the raw yields reconstructed by the TW have been measured from the subtraction between samples with and without target and corrected by purity and efficiency MC corrections. The obtained MC fragmentation cross sections, differential in angle and for each fragment atomic charge Z, were compared to the true MC production cross sections. A remaining discrepancy between MC true and reconstructed cross section has been found to be addressed to the migration between angular bins due to the TW limited granularity with respect to the chosen angular bin width. This discrepancy was corrected with an angular unfolding procedure in the analysis(see Sec. III C), which allowed to dramatically improve the agreement between reconstructed and true MC cross section, expecially in the case of $Z = 6, 7$ fragments for which a narrow angular distribution is expected [22]. The validation of the analysis strategy in the MC, that means background statistical subtraction between samples with and without target, efficiency and purity MC correction to the fragmentation yields and finally angular unfolding procedure to cure the bin migration, confirmed the possibility to apply the same strategy in data. In particular after the background subtraction, the purity correction is applied to correct for the Z charge mis-identification, then the unfolding procedure accounts for the angular bin migration and finally the efficiency correction is applied to account for the not reconstructed fragments. The cross section results will be shown in the Sec. IV.

B. Purity

In this analysis the TW is the only detector able to identify the charge of the fragments using the energy release ΔE in a TW bar and the Tof between SC and TW. The purity is a quantity which is related to the ZID algorithm performances of the TW and depends on the energy loss and Tof resolutions, which in MC are tuned from data, as explained in Sec. III A [23]. To account for the charge Z mis-identification it was needed to introduce a purity correction, which is calculated in MC for each charge and angle, and can be written as:

$$P(Z_{\rm reco}, \theta_{\rm reco}) = \frac{N(Z_{\rm reco} = Z_{\rm true}, \theta_{\rm reco})}{N(Z_{\rm reco}, \theta_{\rm reco})} \quad (5)$$

where $N(Z_{\rm reco}, \theta_{\rm reco})$ is the number of fragments reconstructed by the TW with charge Z_{reco} while $N(Z_{\rm reco} = Z_{\rm true}, \theta_{\rm reco})$ is the number of fragments reconstructed by the TW with charge Z_{reco} equal to the true charge Z_{true} from MC.

The purity correction is applied as a multiplying factor to the fragmentation yield:

$$Y(Z, \theta) = Y_{raw}(Z, \theta) \times P(Z_{\rm reco}, \theta_{\rm reco}) \quad (6)$$

where $Y_{raw}(Z, \theta)$ is the yield subtracted of Eq. 3 before the purity correction application. The obtained $Y(Z, \theta)$ is the one entering the Eq. (1). The purity correction is found to be more than 90% for all the fragment charges Z, with the exception of the case of the Li, for which the purity goes down to the 70%. This drop is due to events with a pair of He fragments entering in a single TW bar cross which release an energy ΔE comparable to the one of a Li, causing a mis-identification of the two He ions in a Li. Two He fragments emitted in a narrow angle is a well known process, in fragmentation physics at these energies, see for example [20], and for the FOOT setup of this analysis is an unavoidable contamination for Li fragments. Only with the trackers of the full FOOT setup [22] it will be possible to identify and separate the two He ions and account for their simultaneous energy release in a TW point. The impact of the purity correction was completely underestimated in the previous work related to the data collected in the GSI campaign of 2019 [23] and the observed discrepancies between the two analysis come from this correction (see Sec. IV), together with the very few statistics collected in that campaign.

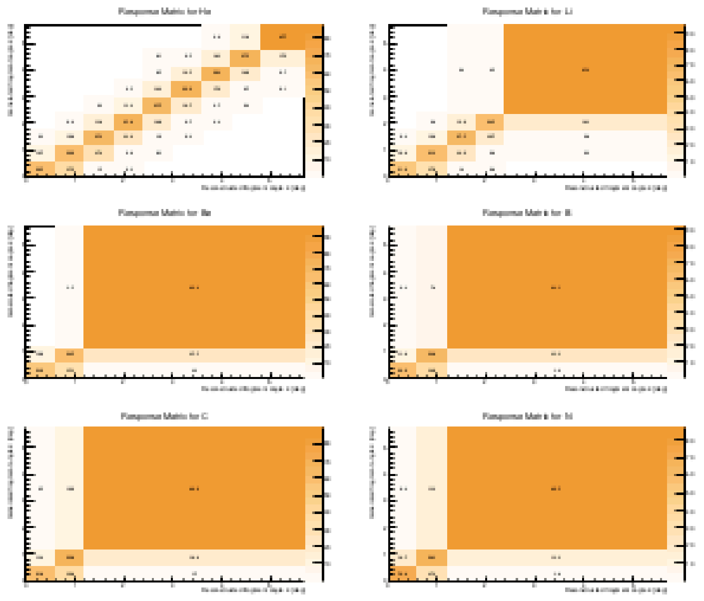

FIG. 3. Response matrices of the different fragments. In each response matrix, only bins where the migration is greater than 0.1% are shown.

C. Unfolding procedure

As already pointed out, the detector effects on angle measurement have to be taken into account when dealing with angular differential cross sections. In particular, Multiple Coulomb Scattering and TW granularity play a major role. To evaluate these effects, the matrix $\theta_{\rm reco} - \theta_{\rm true}$ is built (in the following the *response matrix*), where $\theta_{\rm reco}$ is the angle reconstructed in the analysis while $\theta_{\rm true}$ is the production angle of fragments born in the target (the scattering inside the target resulted to be negligible).

The unfolding procedure is based on a Bayesian iterative algorithm [35] [36] as implemented in RooUnfold [37]. In the unfolding of binned data, the effects of the experimental acceptance and resolution are expressed in terms of a two-dimensional response matrix, C_{ij}, where each element corresponds to the probability of an event in the i-th generator- level bin being reconstructed in the j-th measurement bin. The unfolding algorithm combines the measured spectrum with the response matrix to form a likelihood, takes as input a prior for the specific kinematic variable and iterates using the posterior distribution as prior for the next iteration. The MC FLUKA distribution is used as the initial prior and three iterations are performed. The number of iterations is optimized to balance the unfolding stability with respect to the previous iteration and the growth of the statistical uncertainty. The final choice of three iterations is driven by the minimization of the average correlation factor [38]. The response matrices for the angular distribution of the different fragments are shown in Fig. 3. In order to ensure that the Monte Carlo sample used for the unfolding training is not introducing a bias on the data measurement, a study is performed by changing the pseudo-data distribution. The MC FLUKA angular spectrum

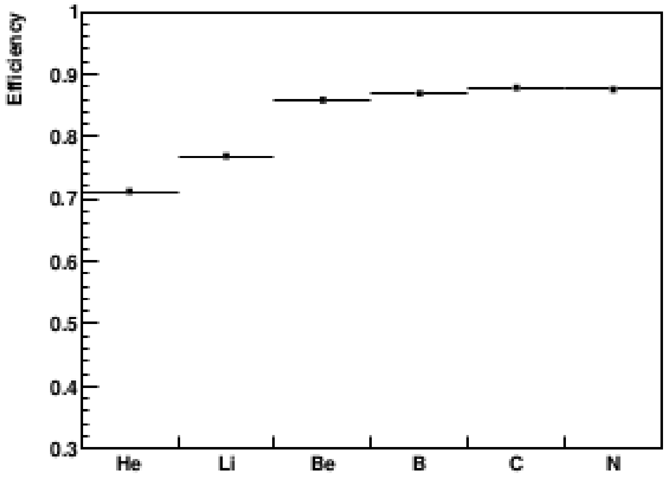

FIG. 4. Efficiencies for each reconstructed fragment of charge Z emitted in the TW acceptance of 5.7°.

is re-weighted using continuous functions to alter the final shape with the same binning. The study confirms that the altered shapes unfolded based on the nominal corrections are preserved within statistical uncertainties.

D. Efficiency

The efficiency for each Z and for each angle θ is computed in order to account for the fragments not reconstructed by the TW detector. Also fragments produced in the TG, within the TW detector acceptance, ($\theta < 5.7°$), but not reaching the TW due to multiple coulomb scattering or fragmentation in air, are contributing to the efficiency computation. In particular, while this last contribution is almost negligible, the impact of the TW reconstruction which discards association of X-Y bars with different Z charge reconstructed, in order to maximize the purity of the charge Z of the TW points has an important impact [23]. The efficiency is defined for each fragment of charge Z_{true} and for each angle θ_{true} as follows:

$$\varepsilon(Z,\theta) = \frac{N_{\mathrm{TW}}(Z,\theta)}{N_{\mathrm{prod}}(Z,\theta)} \tag{7}$$

where $N_{\mathrm{TW}}(Z,\theta)$ are the fragments with charge Z_{true} and emission angle θ_{true} reconstructed by the TW and $N_{\mathrm{prod}}(Z,\theta)$ are the fragments with charge Z_{true} and emission angle θ_{true} produced within the target in the angular acceptance of the TW detector. The efficiencies are shown in Fig. 4 for each Z.

As already mentioned the most important contribution to the efficiency reduction come from the TW reconstruction. And its impact is expected to be bigger for the light fragments like He and Li where more crowdy events cause a bigger probability of mismatch of the Z of two associated X-Y bars, that for this reason are rejected by the TW reconstruction [23].

E. Systematic uncertainties

Several sources of systematic uncertainties were identified in the analysis, both on the detectors involved and in the analysis method. The systematic uncertainties coming from reconstruction at detector level were evaluated changing reconstruction or calibration strategy or parameters used in the reconstruction and propagating the variation through the full cross section analysis and comparing with the default value. Two sources of systematics at detector level have been studied: the impact of the event selection performed using the BM and the requirements on the fragments reconstruction inside the TW.

The former systematic has been studied varying the selection criteria for the BM reconstructed tracks. A tight and a loose selection of the BM hits to be associated to a track, has been implemented and tested to verify the impact on the event pre-selection on the cross section measurements. The impact of this systematic uncertainty was found to be negligible.

Another source of systematic uncertainty is related to the charge reconstruction algorithm in the TW detector. This has been studied varying in the MC simulation the resolutions, within the experimental precision, in ΔE, Tof and in the position measurements that affect the identification of the fragments in MC and thus the efficiencies and the purity evaluation. The only significant contribution was found to be the one related to the He ($< 0.5\%$). To check the impact on the ZID reconstruction also the Bethe-Bloch parametrized curves, extracted from a fit of the plot of ΔE vs Tof at the true MC level, as explained in [23], have been moved within the statistical error. The impact of this variation is again not negligible only for the lighter fragments H and He ($< 0.5\%$). Another systematic studied to look for effects on the purity correction was a more stringent request on the fragment charge Z selection, asking for each point in the ΔE vs Tof plane to be within N sigmas from the closest Bethe-Bloch curve. The impact of this selection is very strong on the available statistics for the background sample and it is not possible to ask for a number of sigmas less than 2. In the end the impact on the purity was found to be of limited impact with respect to the loss of statistics. This can be understood clearly looking at Fig. 2. The different Z charges are already well separated. In the specific case of the Li, where the purity correction has the biggest impact, there is no evident different distribution due to the pair of He ions release with respect to the one of Li. Due to the low statistics of the background sample this systematic results negligible because compatible within the statistical uncertainties with respect to the default. Finally the impact on the ZID coming from the TW calibration strategy was tested. In the TW calibration each ΔE peak is fitted and calibrated to the MC value with a Birks fit [23, 29, 34]. Moving the ΔE fitted mean value within the statistical error an impact which range in the interval [0.1-2]% has been found.

The systematic uncertainty on the unfolding procedure has been assessed by unfolding the MC FLUKA angular distribution using a different unfolding method with respect to the nominal one (Bayesian iterative). The Iterative Dynamically Stabilized (IDS) method [39] has been chosen as alternative method using the same number of iteration. The difference on the unfolded spectra between the two method range in the interval [0.1-3.6]% where the biggest impact is on some angular bin of the heavier fragments.

Finally, the robustness of the reconstruction procedure, including the background subtraction exploiting out of target fragmentation, has been checked. The use of a background subtraction approach, given its statistical nature, introduced an uncertainty in the cross section reconstruction. As reported in Sec. III A, the analysis method was validated looking at the agreement between true and reconstructed MC cross sections after the unfolding procedure. The difference between the true and the reconstructed MC cross sections takes into account all the intrinsic limitations of the adopted strategy mainly due to the absence of tracking detectors in between the target and the TW detector, about 2 m apart. This contribution was found to have an impact for all the fragments in the range [0.3-2.5]% for total cross sections and it can be as high as 10% for angular differential cross sections.

The numerical evaluation of the overall contributions of the systematic uncertainties is shown in the fourth column of Table I and of Table II.

IV. RESULTS

For data analysis, all the six runs of 400 MeV/u ^{16}O on 5 mm Carbon target were considered along with a run without target to perform background subtraction. Three among physics runs were acquired with MB trigger: despite in these runs the interesting share of events can be low, they are very important for two main reasons. Firstly, MB trigger is not affected by biases and its operation is quite robust. Secondly, MB runs are used to tune fragmentation trigger for the relevant beam-target setting. Indeed, during MB runs, trigger thresholds on TW central bars are chosen as a trade off between the rejection of non- fragmentation events while keeping most of Nitrogen fragments which can be affected by a too tight choice of the thresholds. For the other three runs, a mixed trigger setting was chosen, namely all the fragmentation events were acquired along with a fraction of MB events: this means that the data sample contains both FRAG events and MB events (1 out of 10 in this case). However, since the MB trigger rate is much higher than the FRAG trigger rate, in these runs the events are almost equally shared between MB and FRAG and thus they have to be considered as two independent measurements. Data quality checks were performed separately on each run to assess the consistency among data acquired in the same setting. After the successful outcome of such checks all the MB statistics was added together (all the MB runs and the MB part of FRAG runs) and the same was done with FRAG statistics. The background subtraction at yields level is performed after the calculation of $Y_{\mathrm{TG}}/N_{\mathrm{prim,TG}}$ as weighted average of MB and FRAG data samples. After selection cuts discussed in Sec. III $\approx 1.7\times10^6$ MB events and $\approx 6.8\times10^5$ FRAG events (corresponding to more than four million primary particles) were used for the analysis while for the background only $\approx 5\times10^4$ were selected due to the limited amount of statistics without target. Thus, the error on cross section measurements, especially on angular ones, is mainly driven by the error on the sample without target. All the yields in Eq.(1) and in Eq.(4) are considered after the unfolding procedure. In Fig. 5 the elemental cross section for $2 \leq Z \leq 7$ in the relevant polar angle range and velocity range is reported, along with statistics and systematics errors (discussed in Sec III E).

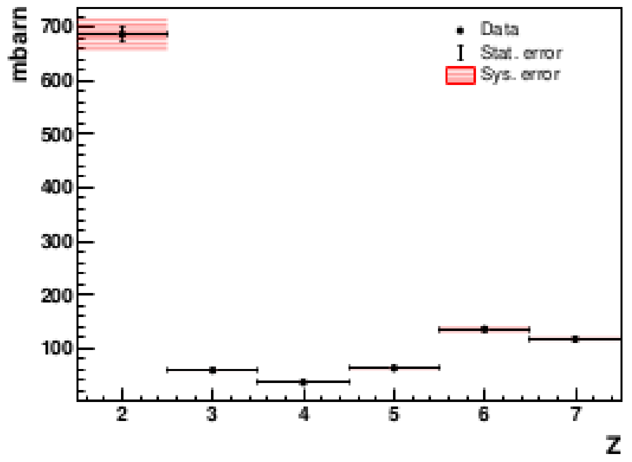

FIG. 5. Elemental fragmentation cross sections for fragments $2 \leq Z \leq 7$.

In Table I the elemental cross sections for He, Li, Be, B, C and N fragments in the velocity range $0.3-0.9$ and integrated in the angle $0^\circ \leq \theta \leq 5.7^\circ$ are reported. Despite the ^{16}O beam was delivered at an energy of 400 MeV/u , the effective energy per nucleon at the target was a bit lower due to previous energy losses and it was estimated by MC simulation to be equal to 393 MeV/u at the center of the target. In Table I, the statistical and systematic uncertainties are reported separately and their weight on the final value is reported. Except for Helium, it is possible to see that the systematic uncertainty it is always lower that the statistical one, which is mainly driven by the limited statistics of the sample without target. As already reported in [23], to our knowledge there are no relevant measurements for He and Li at these energies while there are some for $Z \geq 4$. Moreover, no new measurements were published between [23] and the writing of this work. The obtained elemental cross sections are then directly comparable with our previous measurements, since

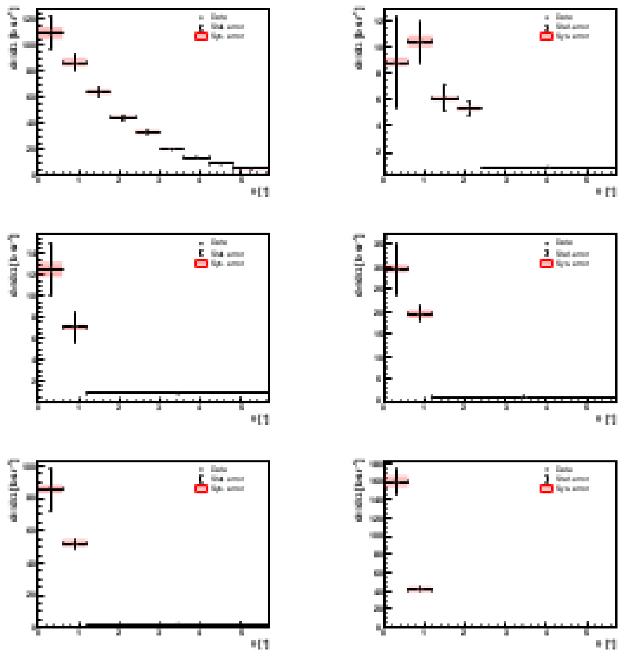

FIG. 6. Angular differential cross sections for fragments $2 \leq Z \leq 7$.

Element	$\sigma \pm \Delta_{stat} \pm \Delta_{sys}$ [mb]	Δ_{stat}/σ	Δ_{sys}/σ
He	$687 \pm 13 \pm 30$	1.9%	4.3%
Li	$59 \pm 3 \pm 2$	5.4%	3.2%
Be	$36 \pm 3 \pm 1$	7.6%	3.2%
B	$63 \pm 4 \pm 3$	5.7%	4%
C	$135 \pm 6 \pm 5$	4.5%	3.7%
N	$117 \pm 6 \pm 4$	5.4%	3%

TABLE I. Elemental cross sections measured in this work. The contribution of the statistical and systematic uncertainties is reported separately. The contribution of the statistical and systematic uncertainties to the final result is visible through the reported relative errors.

the angular acceptance was the same and the velocity range of this work is slightly larger but with a minimum impact on the results. From previous work, the main comparison was performed with [20], a paper providing elemental cross sections within an angular acceptance of $\simeq 7°$ with a 375 MeV/u ^{16}O beam, an energy slightly lower with respect to this work. In particular, only $Z \geq 5$ cross sections were provided, allowing a fair comparison despite the different angular acceptance given the mostly forward production of such fragments. In [23] we concluded that the results seemed to confirm those in [20]. In this work, we confirm our previous measurements regarding Be, C and N while for He, B the result is slightly lower but still comparable within the uncertainties. The biggest difference involves the Li results. As discussed in Sec. III B this is due to the impact of the purity correction not taken into account in the previous work. The effect of the absence of the purity correction in previous work is the one of overestimating the cross sections for those fragments for which the correction is bigger. While the correction is almost negligible for most of the fragments for Li is important due to the events of He ions pairs which release in a TW bars' crossing an energy similar to the one released by a Li, as discussed in III B. The final results for the angular differential cross sections are shown in Table II. To our knowledge, in this case, there are no previous results to compare with. Thanks to the unfolding techniques, we succeeded in reducing the systematic uncertainties on the angular spectrum although the limited statistics of the without target sample gave an important contribution to the statistical uncertainties going from 5% to 20% on average except for a 40% contribution in the first bin of Li. As already mentioned, the number of bins and their width were carefully chosen considering the available statistics in order to have a reasonable number of fragments in each bin.

Z	θ[°]	$\sigma \pm \Delta_{stat} \pm \Delta_{sys}$ [b sr^{-1}]	Δ_{stat}/σ	Δ_{sys}/σ
	$0 - 0.6$	$110 \pm 13 \pm 5$	11.6%	4.3%
	$0.6 - 1.2$	$87 \pm 6 \pm 3$	7.2%	4%
	$1.2 - 1.8$	$65 \pm 3 \pm 2$	5.2%	3.1%
	$1.8 - 2.4$	$45 \pm 2 \pm 1$	4.7%	3.2%
2	$2.4 - 3$	$34 \pm 1 \pm 2$	3.6%	4.4%
	$3 - 3.6$	$20 \pm 1 \pm 1$	4.2%	4.5%
	$3.6 - 4.2$	$14 \pm 1 \pm 0.5$	4.2%	3.5%
	$4.2 - 4.8$	$9 \pm 0.4 \pm 0.3$	4.3%	3.5%
	$4.8 - 5.7$	$5 \pm 0.3 \pm 0.7$	5%	14%
	$0 - 0.6$	$9 \pm 4 \pm 0.3$	40%	3.7%
	$0.6 - 1.2$	$11 \pm 2 \pm 0.4$	15%	4.2%
3	$1.2 - 1.8$	$6 \pm 1 \pm 0.2$	17%	3.1%
	$1.8 - 2.4$	$5 \pm 0.5 \pm 0.2$	9%	3%
	$2.4 - 5.7$	$1 \pm 0.04 \pm 0.04$	5%	4.2%
	$0 - 0.6$	$13 \pm 3 \pm 0.7$	20%	5.3%
4	$0.6 - 1.2$	$7 \pm 1.5 \pm 0.2$	21%	3.2%
	$1.2 - 5.7$	$1 \pm 0.1 \pm 0.03$	9%	3.5%
	$0 - 0.6$	$30 \pm 6 \pm 1$	20%	3.1%
5	$0.6 - 1.2$	$19 \pm 2 \pm 1$	10%	4.7%
	$1.2 - 5.7$	$1 \pm 0.1 \pm 0.05$	7%	4.3%
	$0 - 0.6$	$86 \pm 13 \pm 3$	15%	3%
6	$0.6 - 1.2$	$52 \pm 3 \pm 2$	5.5%	4.3%
	$1.2 - 5.7$	$2 \pm 0.1 \pm 0.08$	5.6%	4.6%
	$0 - 0.6$	$160 \pm 15 \pm 6$	9%	3.9%
7	$0.6 - 1.2$	$42 \pm 3 \pm 3$	6.8%	7.5%
	$1.2 - 5.7$	$1 \pm 0.1 \pm 0.03$	13%	4.4%

TABLE II. Angular differential cross section measured in this work. The contribution of the statistical and systematic uncertainties is reported separately. The contribution of the statistical and systematic uncertainties to the final result is visible through the reported relative errors.

V. CONCLUSIONS

In this work, the analysis for the measurement of the elemental fragmentation cross sections of a 400 MeV/u ^{16}O beam interacting with a 5 mm graphite target has been presented. Notably, we achieved the first measurement of differential angular cross sections for this

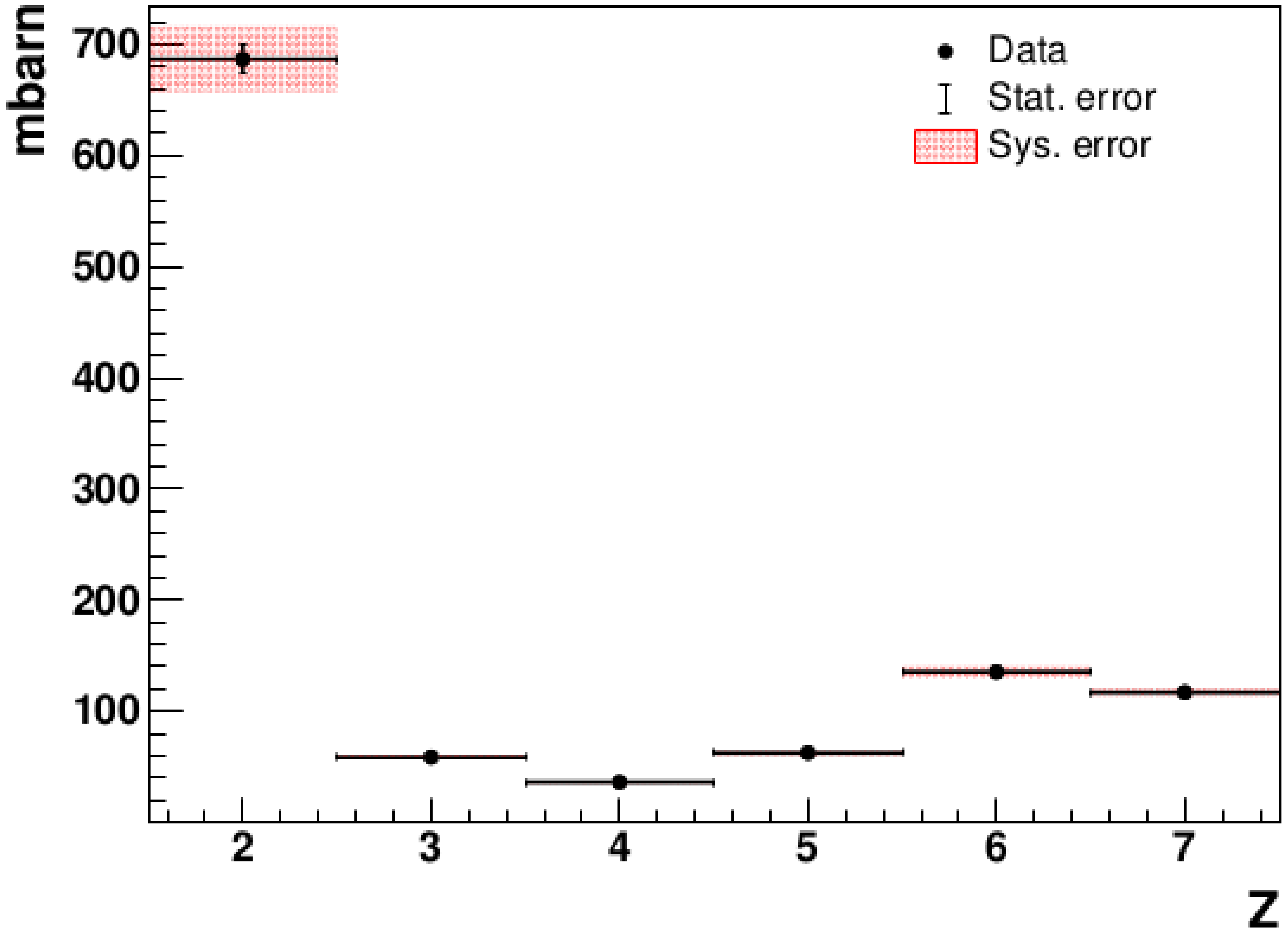

FIG. 5. Elemental fragmentation cross sections for fragments $2 \leq Z \leq 7$.

Element	$\sigma \pm \Delta_{stat} \pm \Delta_{sys}$ [mb]	Δ_{stat}/σ	Δ_{sys}/σ
He	$687 \pm 13 \pm 30$	1.9%	4.3%
Li	$59 \pm 3 \pm 2$	5.4%	3.2%
Be	$36 \pm 3 \pm 1$	7.6%	3.2%
B	$63 \pm 4 \pm 3$	5.7%	4%
C	$135 \pm 6 \pm 5$	4.5%	3.7%
N	$117 \pm 6 \pm 4$	5.4%	3%

TABLE I. Elemental cross sections measured in this work. The contribution of the statistical and systematic uncertainties is reported separately. The contribution of the statistical and systematic uncertainties to the final result is visible through the reported relative errors.

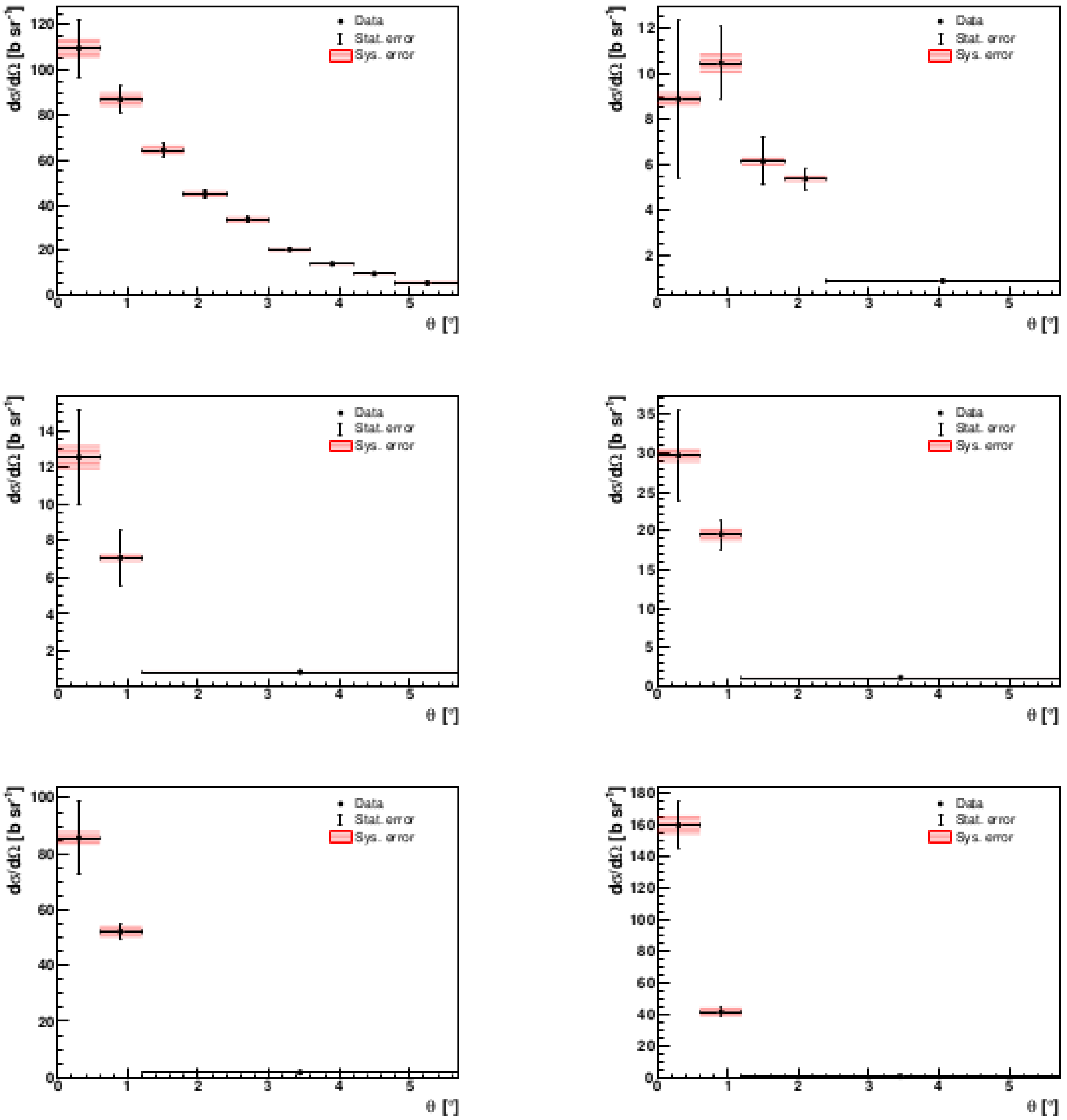

FIG. 6. Angular differential cross sections for fragments $2 \leq Z \leq 7$.

Z	$\theta[^\circ]$	$\sigma \pm \Delta_{stat} \pm \Delta_{sys}$ [b sr^{-1}]	Δ_{stat}/σ	Δ_{sys}/σ
	$0 - 0.6$	$110 \pm 13 \pm 5$	11.6%	4.3%
	$0.6 - 1.2$	$87 \pm 6 \pm 3$	7.2%	4%
	$1.2 - 1.8$	$65 \pm 3 \pm 2$	5.2%	3.1%
	$1.8 - 2.4$	$45 \pm 2 \pm 1$	4.7%	3.2%
2	$2.4 - 3$	$34 \pm 1 \pm 2$	3.6%	4.4%
	$3 - 3.6$	$20 \pm 1 \pm 1$	4.2%	4.5%
	$3.6 - 4.2$	$14 \pm 1 \pm 0.5$	4.2%	3.5%
	$4.2 - 4.8$	$9 \pm 0.4 \pm 0.3$	4.3%	3.5%
	$4.8 - 5.7$	$5 \pm 0.3 \pm 0.7$	5%	14%
	$0 - 0.6$	$9 \pm 4 \pm 0.3$	40%	3.7%
	$0.6 - 1.2$	$11 \pm 2 \pm 0.4$	15%	4.2%
3	$1.2 - 1.8$	$6 \pm 1 \pm 0.2$	17%	3.1%
	$1.8 - 2.4$	$5 \pm 0.5 \pm 0.2$	9%	3%
	$2.4 - 5.7$	$1 \pm 0.04 \pm 0.04$	5%	4.2%
	$0 - 0.6$	$13 \pm 3 \pm 0.7$	20%	5.3%
4	$0.6 - 1.2$	$7 \pm 1.5 \pm 0.2$	21%	3.2%
	$1.2 - 5.7$	$1 \pm 0.1 \pm 0.03$	9%	3.5%
	$0 - 0.6$	$30 \pm 6 \pm 1$	20%	3.1%
5	$0.6 - 1.2$	$19 \pm 2 \pm 1$	10%	4.7%
	$1.2 - 5.7$	$1 \pm 0.1 \pm 0.05$	7%	4.3%
	$0 - 0.6$	$86 \pm 13 \pm 3$	15%	3%
6	$0.6 - 1.2$	$52 \pm 3 \pm 2$	5.5%	4.3%
	$1.2 - 5.7$	$2 \pm 0.1 \pm 0.08$	5.6%	4.6%
	$0 - 0.6$	$160 \pm 15 \pm 6$	9%	3.9%
7	$0.6 - 1.2$	$42 \pm 3 \pm 3$	6.8%	7.5%
	$1.2 - 5.7$	$1 \pm 0.1 \pm 0.03$	13%	4.4%

TABLE II. Angular differential cross section measured in this work. The contribution of the statistical and systematic uncertainties is reported separately. The contribution of the statistical and systematic uncertainties to the final result is visible through the reported relative errors.

Thanks for listening!